nano WILEY

RESEARCH ARTICLE

Fabrication and lubrication performance of sustainable Pickering-like water-in-water emulsions using plant protein microgels

Kwan-Mo You[1] | Brent S. Murray[1] | Simon D. Connell[2] | Anwesha Sarkar[1]

[1]Food Colloids and Bioprocessing Group, School of Food Science and Nutrition, University of Leeds, Leeds, UK

[2]Molecular and Nanoscale Physics Group, School of Physics and Astronomy, University of Leeds, Leeds, UK

Correspondence
Anwesha Sarkar, Food Colloids and Bioprocessing Group, School of Food Science and Nutrition, University of Leeds, Leeds LS2 9JT, UK.
Email: A.Sarkar@leeds.ac.uk

Abstract

Aqueous multiphasic systems have attracted a great deal of interest recently owing to the growing demands of sustainability for the development of stable "oil-free" emulsions, often complicated by their limited stability against droplet coarsening. Although particles may provide ultrastability to water-in-water (W/W) emulsions formed in phase-separating polymer systems, the need for lubrication in such W/W emulsions presents an important challenge for their use in diverse applications. Herein, W/W Pickering emulsions were stabilized by sustainable plant protein (pea)-based microgels (PPM) using starch and xanthan gum as the biopolymers to generate the W/W phase separating droplet structures. The lubricity of these systems was compared with that of parallel systems stabilized by animal (whey) protein microgels (WPM). New results reveal that PPM are more soft and adhesive than WPM and outperform the latter in boundary lubrication performance, in striking contrast to the behavior of the non-microgelled pea or whey proteins. Furthermore, the PPM tend to stabilize a different, less spherical type of W/W droplet than the WPM that may explain the lower friction observed in PPM-stabilized systems. The novel approach of fabricating W/W emulsions stabilized by sustainable microgels opens up new solutions in designing aqueous lubricants for future nutritional and biomedical applications.

KEYWORDS
adhesion, aqrueous lubrication, atomic force microscopy, biopolymer, friction, rheology, W/W emulsion

1 | INTRODUCTION

In recent times, there has been a burgeoning interest in designing eco-friendly multi-compartmental water-based systems[1,2] via thermodynamically incompatible hydrophilic polymers for diverse applications in food,[3,4] cell biology,[5] encapsulation,[6] biocatalysis,[7] and various biomedical applications.[8] However, often these "oil-free" water-in-water (W/W) emulsions suffer from poor stability. Low molecular weight surfactants are not able to offer stabilization because the interfacial tension is already orders of magnitude lower than that of

a typical oil-water (O−W) interface.[2,9] Therefore, Pickering stabilization, that is, using particles as stabilizers, including microgel particles fabricated using animal proteins such as β-lactoglobulin and whey protein[3,10,11] have been used as a promising strategy to improve their stability.[12] By such particles adsorbing to and possibly cross-linking at the water-water (W−W) interface, spinodal decomposition and macroscopic phase separation can be inhibited and water droplets of discrete length scales are maintained.[13]

At the same time, apart from instability problems, a key challenge to address in these "oil-free" W/W emulsion systems is a lack of lubrication performance compared to "oily" systems, including oil-in-water emulsions. Lubrication from oil droplets is often translated into sensory perception described by creaminess and smoothness.[14–16] It is important to characterize both bulk rheological and tribological performance in order to control oral processing,[14,17] which is particularly relevant for food[18] but also oral pharmaceuticals[19] and oral care products.[20] Replacing oil droplets with aqueous solutions can result in diminished lubrication performance unless the water is structured with biopolymers, as widely evidenced in nature-engineered lubricants, such as in tears, synovial fluids, saliva, and so on.[21,22] Recent years have witnessed a growing interest in "green tribology",[23] which strives to find alternatives to environmentally harmful lubricants. Hence, understanding the lubrication behavior of W/W Pickering emulsions is highly topical and could contribute to a new era of green tribology. Up to now, this area is limited to just one study,[3] where it was shown that adsorbing animal (whey) protein-based microgels at W−W interface improved the lubrication performance of a starch-carrageenan biphasic W/W system, as compared to in their absence.

Interestingly, soft, proteinaceous microgels in the size range of hundreds of nanometers have been shown to have an influence on the lubrication between interacting biological surfaces in sliding motion, as in natural joints such as the knee and hip,[24] as well as in food applications.[25] Various microgels from animal or plant-based proteins have been used to design Pickering emulsions. Aggregation of these microgels in the bulk and at interfaces can vary, from a network of aggregated or fused particles that can pack densely at the interface, to discrete microgel particle monolayers at liquid-liquid interfaces.[26] For animal-based protein microgels, whey,[25,27] lactoferrin,[28] and egg white[29] have been investigated for their ability to stabilize Pickering emulsions.

Pickering particles derived from plant proteins have recently attracted much interest owing to growing sustainability demands in technological applications. For example, it is now established that plant-based foods generate half the greenhouse gases as compared to animal-based foods.[30] Whilst studies have focused on the lubrication performance of animal-derived microgels and as Pickering stabilizers, the design of W/W emulsions that are stabilized by sustainable plant particles remains largely unexplored. Although soy protein aggregates,[31] peanut protein microgels[32] and pea protein microgels[33,34] can stabilize O/W emulsions, to our knowledge, no study has investigated the fabrication of W/W emulsions using plant-based particles. More importantly, it has been shown experimentally that aqueous dispersions of plant proteins tend to increase friction compared to their animal protein counterparts.[35,36] Thus, the question remains to what extent can such undesirable frictional behavior be modulated by converting plant proteins to plant protein *microgels*[37] when such microgels are present along with a W−W interface.

Consequently, in this work we fabricate plant protein (pea protein)-based microgels (PPM) for the stabilization of Pickering W/W emulsions. We show the unique ability of PPM to offer higher boundary lubrication properties compared to WPM by virtue of their softer character and more adhesive properties. In addition, the PPM tends to stabilize less spherical W/W droplets than with WPM, which may also contribute to the enhanced lubrication properties with PPM. This knowledge was achieved via the use of a comprehensive suite of multiscale characterization techniques such as rheology, tribology, quartz crystal microbalance with dissipation monitoring, light scattering, confocal laser scanning microscopy, cryogenic scanning electron microscopy and atomic force microscopy. The findings present a novel route to the design of green, stable aqueous lubricants for the future.

2 | RESULTS AND DISCUSSION

Microgels fabricated using proteins, polysaccharides, lipids and synthetic polymers have attracted significant research attention recently due to their outstanding aqueous lubrication performance in various food, biomedical and pharmaceutical applications.[9,17,42–43] Recent studies have shown that microgels can be fabricated from various food proteins, from both animal and more sustainable plant sources, using just physical crosslinking processing such as heat and pH changes,[19,25,44] that is, with the commercial advantage of not using additional chemical crosslinking agents. However, the lubrication performance of microgels, especially those fabricated from plant proteins at the W-W interface remains largely unexplored.

Firstly, we checked the ability of PPM to stabilize Pickering W/W emulsions formed from gelatinized starch (GS) and xanthan gum (XG) mixtures at various concentrations
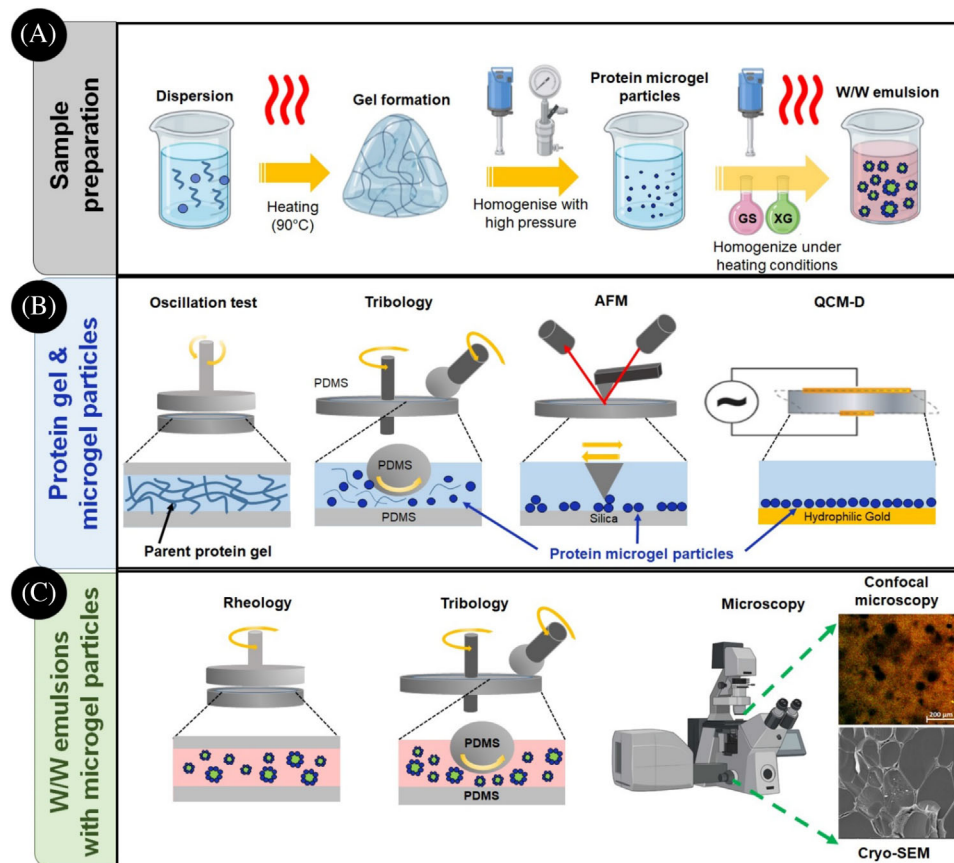
FIGURE 1 Multiscale methodology. A) Sample preparation of whey and pea protein microgel particles (WPM and PPM, respectively) and water-in-water (W/W) emulsions stabilized by the microgel particles. B) Characterization of protein hydrogels and microgel particles; dynamic viscoelasticity during and after gel formation; tribology with polydimethylsiloxane (PDMS) ball-and-disk tribometer; imaging of microgels using atomic force microscopy (AFM); quantification of film formation on gold surface using quartz crystal microbalance with dissipation monitoring (QCM-D). C) Characterization of W/W emulsions from xanthan gum (XG) + gelatinized corn starch (GS) mixtures stabilized by microgel particles via bulk viscosity; tribology; confocal scanning laser microscopy (CLSM) and cryogenic scanning electron microscopy (Cryo-SEM).

(Figure 1A), for comparison with WPM.[3,38] It was also important to understand how PPM compares to WPM in terms of tribological performance, as it is known that non-microgelled pea protein jams the tribo-contacts and tends to increase friction significantly as compared to its whey protein counterpart.[35]

Firstly, the rheological, tribological, and surface properties of the microgels on their own were characterized via a quartz crystal microbalance with dissipation monitoring (QCM-D) on hydrophilic gold substrates, combined with measurement of surface adhesion via an atomic force microscope (AFM), as illustrated schematically in Figure 1B. Next, we explored the behavior of PPM in the W/W emulsion systems. We also tried to answer questions about how the microstructure of the droplets might affect frictional properties using cryogenic scanning electron microscopy (cryo-SEM) and confocal laser scanning microscopy of the water droplets (Figure 1C).

2.1 | Rheological features of the parent protein gels

The dynamic shear rheological properties of the parent gels from which the microgels were formed were measured, with the assumption that the mechanical properties of the microgels themselves are not too disparate.[39] Figures 2A,B show the results of oscillatory shear rheometry experiments performed on whey and pea protein hydrogels where in situ gel formation (via heating and cooling) was performed between the parallel plates of the rheometer, as illustrated in Figure 1B. Interestingly, there were marked differences in the kinetics of development of the storage (G') and loss (G'') between the whey and pea proteins (see Figures S1A and S1B, respectively). The gelation point was taken as where $G' > G''$. This was at a much higher temperature (90°C) for whey protein (Figure S1B), whereas gelation of pea protein appeared to be a two-step
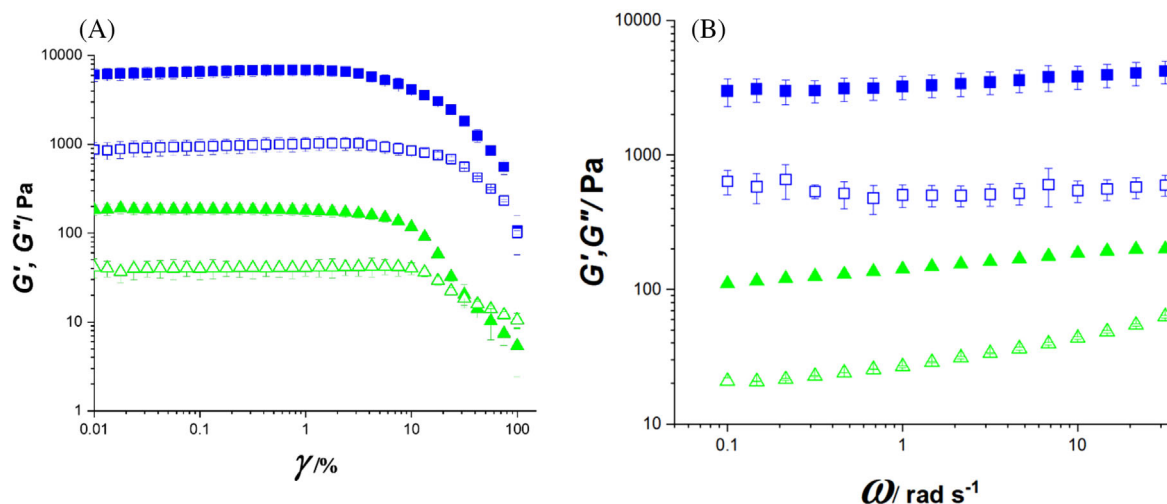
FIGURE 2 Bulk viscoelasticity of parent hydrogels. Oscillatory shear rheometry performed on 12.0 wt% whey (■) and pea protein hydrogels (▲). Closed symbols = G', open symbols = G". A, Strain (g) amplitude sweeps at $\omega = 6.28$ rad s^{-1}. B, Oscillatory frequency sweeps at g = 1%. Means and standard deviations are reported for at least three measurements on experiments performed in triplicates ($n = 3 \times 3$).

process, most likely involving a solubilizing step at around 60°C, followed by the onset of the most rise in G' at around 70°C (Figure S1B). However, at the same protein concentration, the end result was a weaker (lower G') gel for the pea protein.

In terms of the strain dependence of G' at $\omega = 6.28$ rad s^{-1}, both the protein gels showed almost a plateau in G' at low strain but beyond a similar region of higher strain for both gels, G' reduced considerably, indicating a weakening of the structure. However, it should be noted that in the plateau regions at low strain, G' was considerably higher (~80 times) for the whey than the pea protein gels. The pea protein gels also showed an increase in G" over G' at higher strains unlike with whey protein, although the data from different samples was quite scattered beyond this cross-over region. Figure 2B shows the result for frequency sweeps at a strain amplitude of 1%, within the plateau region for both gels. Strong gel behavior may be defined as a frequency-independent plateau in G' where G' ≫ G".[40] Both G' and G" were independent (within experimental error) of ω for the whey protein, whilst the pea protein gels seemed to show slight strain hardening and a convergence of G' and G" up to $\omega = 40$ rad s^{-1}, though G' was still lower than for the whey protein gel.

Overall then, the whey protein gels can be considered as much stronger and stiffer than the pea protein gels. This is not so surprising given that there is widespread evidence that covalent disulfide bonding is a major contributor to the gelation of whey protein, whereas it has not been shown to play a major role for pea protein gelation.[41] Cystine (two cysteine residues linked together via a disulfide bond) is found at twice the concentration in whey protein than in pea protein,[42] thus contributing to increased disulfide bonding in the former and hence the higher gel strength in whey protein gels.

2.2 | Microstructural, bulk and surface properties of microgels

Having characterized the deformability of the bulk gels, the properties of the corresponding microgels were studied, in particular the interactions with surfaces in order to explain the tribological features in the boundary regime. In this regime surface interactions are particularly important to the mechanism behind frictional dissipation.[43] AFM allowed structural characterization of the submicron-sized WPM and PPM, shown in Figures 3A1 and 3B1, respectively. Both WPM and PPM led to large instabilities when using peak force tapping mode, therefore contact mode was employed. Topographical images of the microgels (Figures 3A1 and 3B1) deposited on a silicon surface revealed a range of sizes of spherical shaped particles as well as small clusters that appeared to contain two to six individual particles. The surfaces of both WPM and PPM appeared to be relatively smooth, in agreement with measurements elsewhere on proteinaceous[39] and non-proteinaceous microgels.[44] Using dynamic light scattering, microgels made from 12.0 wt% WPM and PPM showed a narrow size distribution with a single peak in the size range of 100–1000 nm and the average hydrodynamic diameters (D_h) were 86 ± 4 and 180 ± 6 nm, respectively, with a polydispersity index < 0.25 (Figures 3A2 and 3B2). The particle size distribution was also quantified in the topographic images using the particle analysis function Nanoscope Analysis v1.9 which gave values of 90.0 ± 2
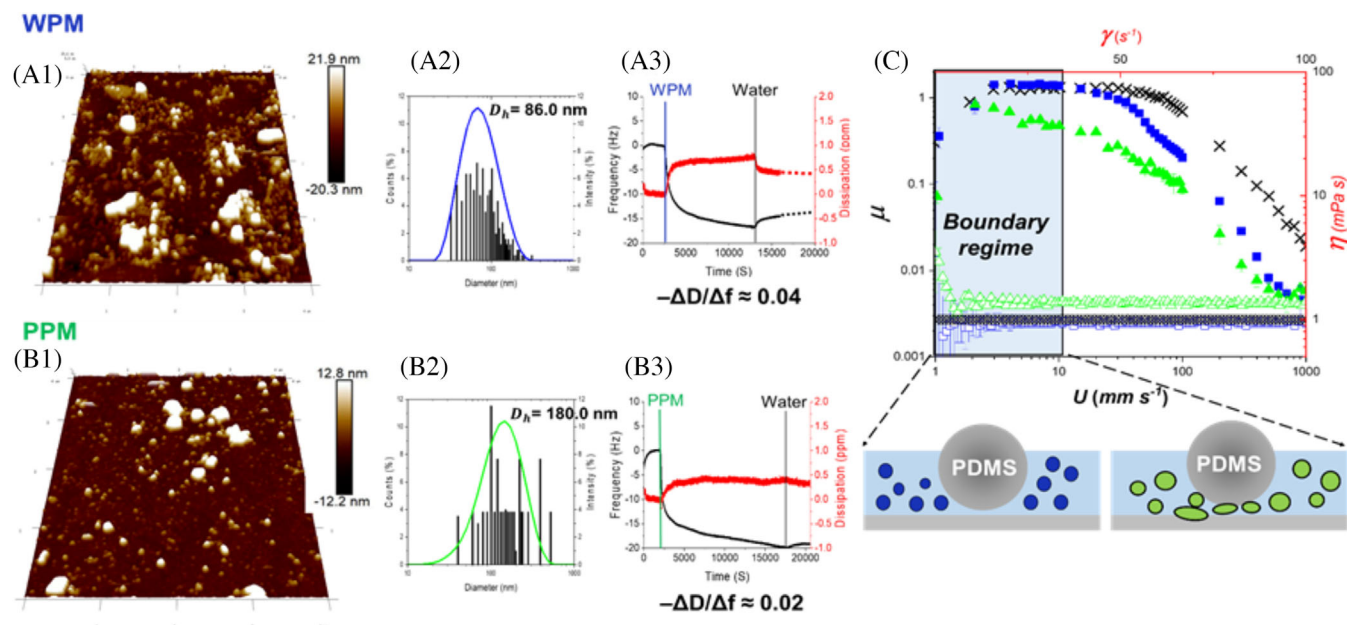
FIGURE 3 Structure and performance of microgels in the bulk phase. Three-dimensional topographic images of microgels deposited on a silicon substrate, as obtained by contact mode AFM for WPM (A1) and PPM (B1). Histogram plots showing the particle size distributions obtained from the AFM images for WPM (A2) and PPM (B2). Superimposed on figures A2 and B2 are the corresponding particle size distributions obtained via DLS. Mean frequency shift (Δf, —) and dissipation change (ΔD, —) are obtained using QCM-D for 0.05 vol% WPM (A3) and PPM (B3) on gold sensors. The final values of $-\Delta D/\Delta f$ (before rinsing) are also given. The vertical line indicates the time at which the system was rinsed with MilliQ water. Mean apparent visosities (η) versus shear rate ($\dot{\gamma}$) of WPM ($\square$) and PPM ($\triangle$) are shown in (C). Mean friction coefficient (μ) versus entrainment speed (U) of WPM ($\blacksquare$), PPM ($\blacktriangle$) and water (X) between PDMS surfaces are also shown in (C) with statistical differences in μ reported in Table S1A. Also shown are schematic illustrations of the proposed state of the WPM (blue) and PPM (green) during these measurements where size and shape of the microgel particles are informed by AFM, DLS and rheology results. Error bars represent standard deviations for at least three measurements on experiments performed in triplicates ($n = 3 \times 3$). AFM, atomic force microscopy; PPM, protein (pea)-based microgels; WPM, (whey) protein microgels.

and 178.4 $\pm$ 4 nm for WPM and PPM, respectively, also shown on Figures 3A2 and 3B2. All these size values were similar to those reported previously for these types of microgels.[3,34]

QCM-D was used to try to understand the adsorption kinetics of the microgels at the W-W interface using hydrophilic gold surfaces, plus the mechanical properties of the microgel films at the surface. When either of the WPM or PPM was added at 0.01 vol%, a substantial decrease in frequency (f), $|\Delta f| = 15$ to 20 Hz occurred over 3 hours, with an increase in dissipation (D) (Figures 3A3 and 3B3), signifying protein adsorption. The changes in $|\Delta f|$ and D and were slower for PPM than WPM and for both the adsorption appeared to be somewhat slower as compared to that observed for the corresponding non-microgelled protein.[35,36] This indicates slower adsorption of the protein microgels than the free protein (as expected) but also slow structural changes in the film of microgels after their adsorption. After nearly 12,500 seconds for WPM and 17,500 seconds for PPM, the $|\Delta f|$ and D values were still changing very slowly but the aqueous phase was then exchanged for water to check for reversibility of

adsorption. Only a small fraction of the changes in $|\Delta f|$ and D values on adsorption was reversed, particularly for PPM, suggesting that most of the microgel material was irreversibly adsorbed. The adsorbed hydrated mass was calculated using Voigt's model, since D also increased rapidly as a function of time, rendering the Sauerbrey model invalid.[45] Figures S2A and S2B show that the calculated hydrated mass of WPM was nearly half of that of the PPM. This might be attributed to the 2$\times$ lower size of the WPM particles compared to PPM. Also, it is important to highlight that the % desorption after the rinsing step was significantly higher in the case of the WPM (16%) as compared to that PPM (5.2%), suggesting that PPM had a higher affinity than WPM for the gold surface. The differences in adsorption and desorption are schematically illustrated in Figure S2. In non-microgelled systems, the hydrated adsorbed mass of whey protein and pea protein on the same substrate has been found to be similar, but when the proteins are thermally-treated[36] the amount of whey protein adsorbed was approximately half that of pea protein, that is, as observed here for the thermally treated microgels (see Figure S2). The adsorbed mass of a protein molecule

(mono)layer is typically 2 to 3 mg m^{-2},[46] thus the adsorbed hydrated mass of the microgels was apparently similar. This suggests that the coverage of the microgel particles on the gold surface, irrespective of the microgel type, was far from a complete monolayer and must be extremely patchy, or the particles very flattened out on adsorption.

The final values of the ratio of dissipation to frequency , -ΔD/Δf , that is, at the end of the adsorption time studied, were calculated: 0.04 for WPM and 0.02 for PPM. The value of −ΔD/Δf characterizes the "degree" of viscoelasticity: higher values represent more viscous and less elastic films, where the time to dissipate energy is increased[22,36] By this measure, although the parent whey protein gel may be more rigid than the pea protein gel, the adsorbed PPM layer is apparently more rigid and less viscous than the adsorbed WPM layer. This seems to agree with the lower tendency for the PPM particles to desorb on exchange with water, so that they appear to be more rigidly adhered to gold surface. This greater adhesion was also confirmed by AFM measurements (Figures S3A and 3B), which showed a 9× higher adhesion force with the silicon AFM probe for the PPM as compared to WPM. Thus it would appear that although PPM microgels might be softer, they are more able to slowly restructure (possibly flattening out, interpenetrating and cross-linking with each other) to form an adsorbed film that becomes more rigid and more strongly adhering to the surface. In contrast, the individual WPM particles may be more rigid but because of this they are less able to cross-link with neighboring WPM at the interface and so cannot form such a resilient film, as schematically illustrated in Figure S2B.

It is worth noting that a relatively low concentration of microgel particles (2.0 vol%) was used to make the W/W emulsions. Hence, as one might expect, the apparent viscosity of the microgel dispersions themselves was negligible and did not vary between the two microgel types: both WPM and PPM at 2.0 vol% showed Newtonian fluid characteristics with viscosity ≈ 1 mPa s (Figure 3C). Thus, the likelihood of the microgels contributing to the viscosity of the W/W emulsions stabilized by the microgels can be considered negligible. It is important to note that non-microgelled whey protein offers better lubricity than pea protein, whereas the latter has been demonstrated to jam the contacts and increase boundary friction between polydimethylsiloxane (PDMS)-PDMS surfaces.[35] Therefore, a key factor was to investigate the differences in lubrication performance of these two proteins when present as microgels (see Figure 3C for results). As expected, water showed minimal reduction in the friction coefficient (μ) at very low entrainment speed (U) in the boundary regime (at U < 5 mm s^{-1}) followed by a reduction of μ in the mixed regime (U = 100–1000 mm s^{-1}), in line with pre-

vious findings.[25] Both WPM and PPM showed a more marked decrease in μ with an increase in U. Strikingly, PPM gave a significantly lower μ in the boundary regime compared to WPM and indeed was lower across the entire experimental window ($p < 0.05$) (see statistical differences in Table S1A). Thus, converting pea protein into PPM converts it from being high friction-generating material to a lubricating system that outperforms WPM, exactly opposite to the case of the non-microgelled proteins where μ for whey protein << pea protein.

To sum up, both WPM and PPM appear to enter the gap between ball and disk and form a hydrated film that helps to separate the tribo-surfaces and reduce friction. However, the WPM particles, that we assume to have a rigidity G' two orders of magnitude higher than the PPM (see Figure 2A), because they are less deformable, less hydrated and easier to desorb in the tribological regime than the PPM, are less able to form a coherent film that keeps the surfaces apart (see schematic in Figure 3C).

2.3 | Water-in-water emulsion systems

Having demonstrated that PPM alone reduces friction more than WPM alone, we investigated whether the same effects occur when the microgels are adsorbed at the W-W interface of the GS + XG phase separating biopolymer system.[3,11] Figure 4 shows the phase diagram of GS + XG mixtures, illustrating the concentration regions where the system is mono- or biphasic. The diagram is typical of others published elsewhere, though details vary slightly due to the variations in the molecular weight distributions of the polysaccharides, due to their origin and processing. Mixtures that showed no phase separation after 2 months of storage were considered to lie in the monophasic region.

The apparent viscosity of the upper, xanthan-rich phase separated layer in various concentrations of the mixtures (0.1 wt% XG + 1.0 or 2.0 wt% GS; 0.2 wt% XG + 1.0 or 2.0 wt% GS; 0.3 wt% XG + 1.0 and 2.0 wt% GS) was measured and compared the viscosity of the corresponding pure XG phases, (i.e., 0.1, 0.2 and 0.3 wt% XG), as shown in Figure 4B. Figure 4C confirms that the viscosities of these upper layers and the corresponding pure XG solutions were almost identical for all mixtures tested, highlighting that the phase separation resulted in an almost pure XG-rich phase at the top. This is in close accordance with the results observed for GS mixed with other polysaccharides, including κ-carrageenan, guar gum, locust bean gum, and other galactomannan gums.[3,11,47] The other, lower phase, may therefore be fairly safely assumed to be mainly starch-rich. The W/W emulsions that showed no phase separation within 1 week were chosen for further microstructural, rheological and tribological analyses.
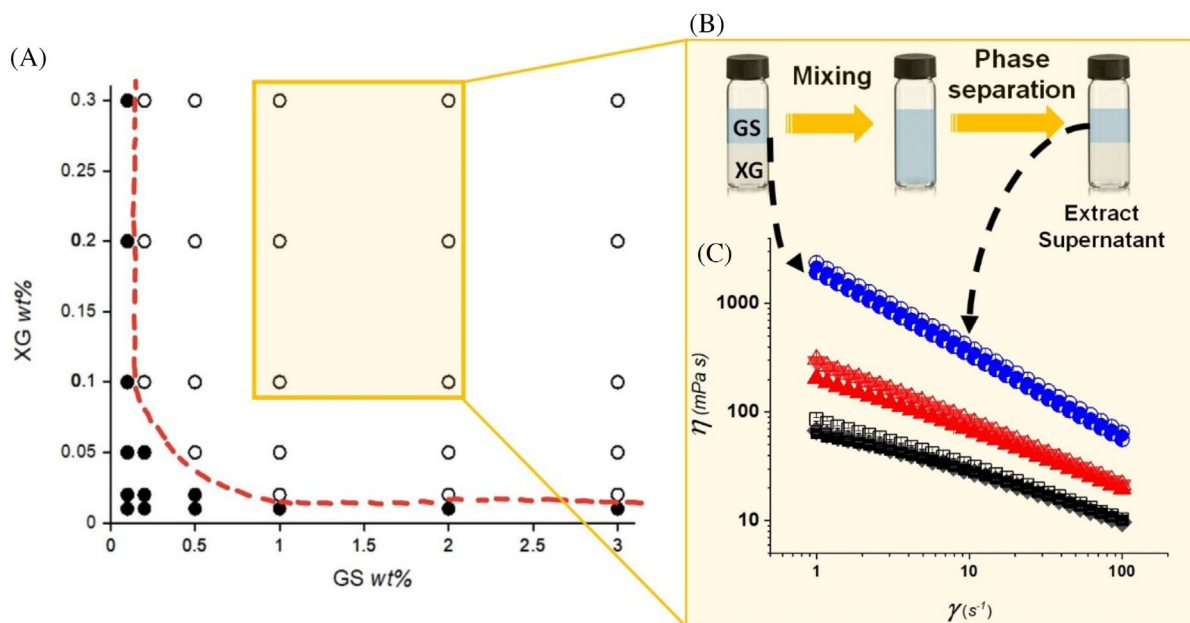
FIGURE 4 Phase diagram and rheological behavior of biphasic systems. Phase diagram (A) of the xanthan gum (XG) + gelatinized starch (GS) system and viscosity curves (B) of mixtures and their corresponding separate phases. In (A), the estimated binodal is shown by the dashed red line (---) and the single phase and biphasic regions are indicated by the filled (●) and unfilled symbols (○), respectively. (B) Schematic diagram of the sampling method to confirm phase separation. (C) The mean apparent viscosity (η) as a function of shear rate ($\dot{\gamma}$) for XG alone at 0.1, 0.2, and 0.3 wt% (■, ▲, and ●, respectively); the upper phase of the phase separated mixtures of 0.1 wt% XG + 1.0 wt% GS (□), 0.1 wt% XG + 2.0 wt% GS (◆), and 0.2 wt% XG + 1.0 wt% GS (△), 0.2 wt% XG + 2.0 wt% GS (▼), and 0.3 wt% XG + 1.0 wt% GS (◯) and 0.3 wt% XG + 2.0 wt% GS (◖). The error bars represent standard deviations for at least three measurements on experiments performed in triplicates ($n = 3 \times 3$).

2.3.1 | Microstructure of microgel-laden W/W emulsions

The microstructure of the W/W emulsions formed from 2 wt% GS + 0.2 wt% XG in the presence and absence of WPM or PPM was monitored across a range of length scales. To our knowledge, only one previous study has shown cryo-SEM evidence of WPM at the interface of W/W emulsion droplets and none with PPM.[3] (Cryo-SEM remains the standard technique to visualize microgels at the oil-water interface in the case of oil-in-water emulsions[27,48,49]) Cryo-SEM observations at 10,000× magnification (Figures 5A1-3 and 5B1-3) revealed the separated GS- and XG-rich regions as a "nested architecture", with a fairly uniform distribution of polyhedral volumes. We assume that these structures are the water droplets that form, rich in one of the two biopolymers. The thickness of the lamellar region separating the water droplets containing interstitial WPM or PPM (see zoomed images in Figure 5 and Figures S4A and 4B) appears to be in the range of hundreds of nm, which roughly corresponds to the microgel particle sizes reported in Figures 3A2 and 3B2. Many of the particles seem to be aggregated in the bulk phases, but a major fraction of the PPM does appear to be situated at the interface. Therefore,

this seems to be the first evidence that PPM can stabilize W/W droplets similar to their stabilization of O/W droplets, which has been previously reported.[34,48] Note that there do seem to be differences between the droplet microstructure stabilized by WPM (Figure 5A1) and PPM (Figure 5B1). In the presence of WPM, more polyhedral water cells with microgels are evident, for example, in the zoomed-in region of Figure 5A2. Of more importance, the microgels are clearly evident at the interface, for example in Figure 5A3. The PPM systems seem to show a similar but more "broken" network structure, with the shape of water droplets appearing more irregular and non-uniform than those stabilized by WPM, as seen in Figure 5B2 and the aggregated network of PPM at the W/W interface was observed in Figure 5B3.

Microgels could affect the characteristics of W/W emulsions through various mechanisms, for example, particle−solvent interactions, osmotic pressure gradients, particle−particle interactions and particle-interface interactions.[50] Taking these in turn, the microgels may change their particle size (swelling or shrinking) according to which of the two phases in they are located and the osmotic pressure of these phases, which in turn will vary according to the local evolving biopolymer concentrations. At the same time, the kinetics of evolution of the phase
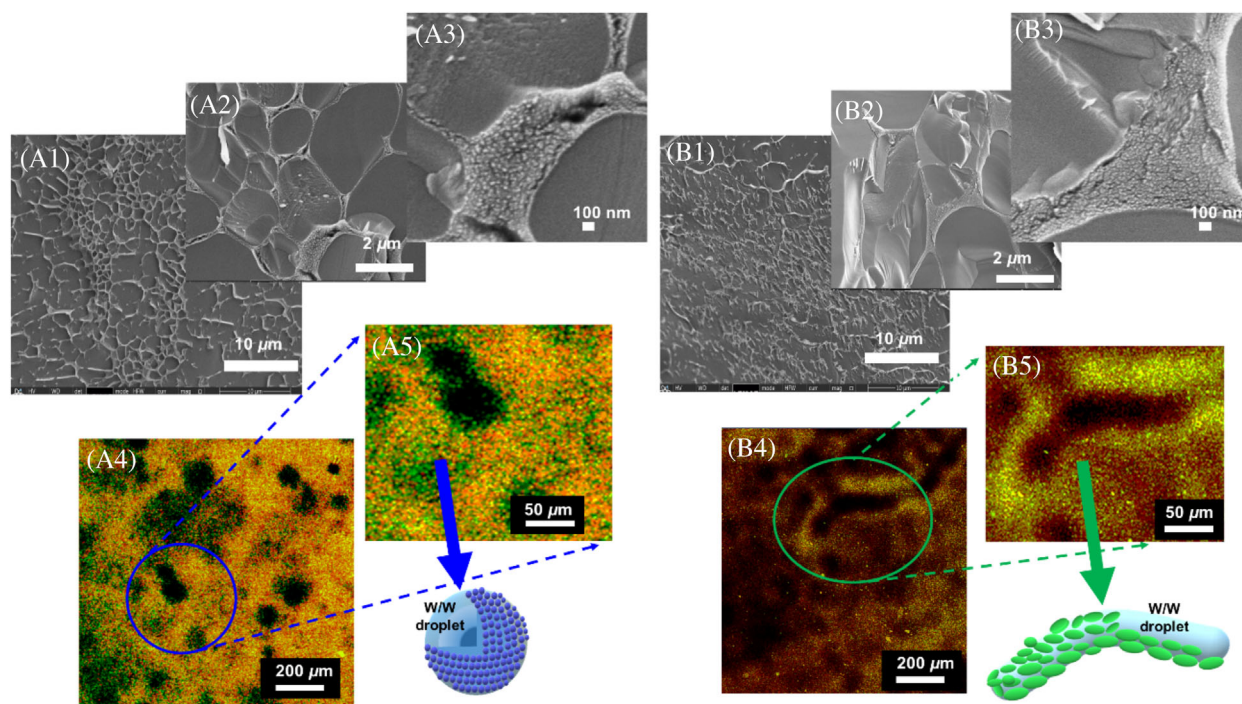
FIGURE 5 Microstructure of W/W emulsions. Cryo-SEM images at different magnifications of 2.0 wt% GS + 0.2 wt% XG W/W emulsions with WPM (A1-A3) and PPM (B1-B3). CLSM micrographs at two different magnifications of the same systems with WPM (A4 and A5) WPM and PPM (B4 and B5) are also shown. GS, WPM and PPM were fluorescently labelled with Rhodamine B ($\lambda \approx 568$ nm, yellow/orange), Acridine Orange ($\lambda \approx 525$ nm, green), and Fast green ($\lambda \approx 633$ nm, green), respectively. The schematics alongside the confocal images illustrate the proposed differences in microstructure of WPM and PPM surrounding the water droplets. PPM, protein (pea)-based microgels; WPM, (whey) protein microgels.

separating structures will be affected by the propensity of the microgels to rapidly adsorbed to the W/W interface and the strength of the attractive interactions between them, causing them form a more continuous and thick microgel layer at this interface. Connected with this is the deformability of the microgels, since softer, more deformable microgels may be able to "unfold", change their shape and form a contiguous microgel layer more quickly and more easily.[51] The greater the magnitude of the interfacial tension (although all the tension values will be low) will also add to the strength of the driving force causing microgel adsorption and unfolding, whilst a higher tension will push the evolving phase separating discontinuous phases structures to adopt more spherical shapes.[52] Gonzalez-Jordan, Nicolai and Benyahia[53] showed that by using heated solutions of β-lactoglobulin under various conditions, one might fabricate protein fibrils, microgels or fractal aggregates. The effect of protein particle morphology was thus important to dictate the shape of the water droplets, but also the stability of W/W emulsions. Unfortunately, we are not yet in a position to define the relative balance of these different mechanisms, whereas our focus is on the practical implications for the lubricity effects.

Confocal laser scanning microscopy (CLSM) of the W/W emulsions provided further information about their microstructural features, free from the possibility of freezing-related artefacts introduced via the sample preparation procedures of cryo-SEM. While cryo-SEM revealed the fine structure of the emulsions and in particular resolved the microgels at droplet boundaries (Figures 5A3 and 5B3), CLSM showed the overall structure at larger length-scales, the even distribution of all components. For clarity, we particularly imaged the larger water droplets (Figures 5A4 and 5A5). Water droplets appeared as dark, unstained areas completely surrounded by WPM (stained with Acridine Orange (AO), that was represented by a green color) whilst the surrounding aqueous phase appeared yellow/orange due to GA stained with Rhodamine B, plus any excess WPM present in this phase. The xanthan was unstained and therefore was largely present in the dark water droplet regions. This confirms the ability of WPM to act as good Pickering stabilizers of W/W emulsion systems[4,10,54] (see Figure S5 for additional CLSM images). Additionally, we mapped the fluorescence intensity due to AO near the W-W interface of droplets and it was fairly evident that the fluorescence intensity (and therefore WPM) was more concentrated in the vicinity of the interface, apparently both inside and outside the droplets, although the resolution is not really sufficient to pin the location of the interface this accurately. Even

more clearly Figure S6 shows the sharp cut-off in AO fluorescence intensity at the water/water phase boundary, further supporting the notion of WPM particles at the interface, in line with Figure 5A3, which shows a similar distribution of microgels at the interface of finer emulsion droplets. It is worth emphasizing that the green fluorescence intensity is still fairly high in the area outside the large droplet. This is believed to be linked to both smaller WPM-coated water droplets as well as unabsorbed microgels in this continuous phase region, which is common in any Pickering emulsion systems, that is, there are always excess unabsorbed particles present. The PPM-loaded W/W emulsions show a different architecture (Figure 5B4). Numerous non-spherical water regions appear to be surrounded by green (Fast Green-stained) PPM (see zoomed image with schematic in Figure 5B5) but here the water droplets have a more deformed shape, reminiscent of spinodal decomposition structures. One might question the apparent difference in size of the droplets observed between Cryo-SEM and CLSM images. The cryo-SEM specifically focused on lower-sized droplets to allow visualization of the droplets together with the interfacial microgels (Figure S4). In addition, the sample preparation (free-fracture) may cause significant changes in the size of the droplets, whereas sample preparation is minimal in the case of CLSM and one necessarily focuses on larger sized droplets due to the lower resolution of CLSM and to avoid blurring due to Brownian motion of the droplets. The next question is whether these different structures perform differently in rheological and tribological regimes and this is addressed below.

2.3.2 | Rheological properties of Pickering-like W/W emulsions

Since the lubrication properties of biopolymeric systems are often determined by their bulk viscosity, particularly in the high shear rate ($\dot{\gamma}$) regimes,[39,55] the apparent viscosities (η) of the W/W emulsions were measured, prepared with 2.0 vol% WPM or PPM at lower (1.0 wt% GS + 0.1 wt% XG) and higher (2.0 wt% GS + 0.2 wt% XG) biopolymer concentrations. The results are shown in Figures 6A1 and 6B1, respectively, alongside controls of the same concentrations of the pure samples of GS and XG. Looking first at the W/W emulsions prepared without microgels, the emulsions were rheologically different to either GS or XG alone, and had non-Newtonian, shear-thinning properties at both concentrations.

At the lower biopolymer concentration (1.0 wt% GS + 0.1 wt% XG), the viscosity of the emulsion $\eta_{emulsion}$ appeared to be much closer to the viscosity of the GS (η_{GS}) than that of the XG (η_{XG}) at all $\dot{\gamma}$ (Figure 6A1).

However, when the concentrations were doubled, $\eta_{emulsion}$ was considerably higher than the corresponding values of η_{XG} or η_{GS} alone, as might be expected from the added structuring of water droplets to the system as observed in Figure 5. In the case of microgel-laden W/W emulsions, as seen in Figure 6 A1 and B1, the microgels enhanced $\eta_{emulsion}$ significantly, compared to the systems without microgels. It is noteworthy that the systems with WPM had a higher $\eta_{emulsion}$ than the ones with PPM at lower $\dot{\gamma}$. This might reflect the greater amount of structuring in the WPM systems evident in the cryo-SEM images (Figure 5). The adsorbed layers of PPM are possibly easier to deform under shear (visible even in the cryo-SEM images) and this inhibits interactions between the droplets and leads to lower $\eta_{emulsion}$ overall than with WPM.

2.3.3 | Lubrication performance of Pickering W/W emulsions

Figures 6A2 and 6B2 show the evolution of friction coefficient (μ) as a function of entrainment speed (U) of the W/W emulsions at the lower and higher biopolymer concentrations, respectively, stabilized by WPM or PPM and alongside the corresponding results for just GS and XG alone. Figure 6A2 shows that the behavior of the W/W emulsions without microgels at the lower biopolymer concentration (1.0 wt% GS + 0.1 wt% XG) is totally different compared to the corresponding GS and XG. The friction coefficients of the W/W emulsions ($\mu_{emulsion}$) in mixed and hydrodynamic regimes were much lower than those for GS (μ_{GS}) or XG (μ_{XG}) alone—although XG seemed to dominate the behavior in the boundary regime. Without microgels at the higher biopolymer concentration (2.0 wt% GS + 0.2 wt% XG) $\mu_{emulsion}$ in the boundary regime showed a rather similar trend as with the lower concentration of biopolymers (Figure 6B2), but in hydrodynamic regime ($U > 500$ mm s^{-1}) $\mu_{emulsion}$ seemed to be closer to that of μ_{GS}.

One key question is whether or not the water droplets became entrained and formed a hydration film in the contact region between the ball-and-disk.[38] Considering the reduction of friction observed in Figure 6, it is certain that the droplets were entrained but most likely deformed under the tribo-shear, since the such large non-deformed droplets (Figure 5) would not be able to enter the contact zone, where the film thickness is usually of the order of tens to hundreds of nanometers.[15] You, Murray and Sarkar[3] demonstrated that the tribological behavior of such water droplets is governed by their size, morphology and volume fraction, depending on the biopolymer concentration. Here the higher biopolymer concentrations seem to give larger droplets and droplets with more non-spherical shapes, whereas the lower concentrations seem
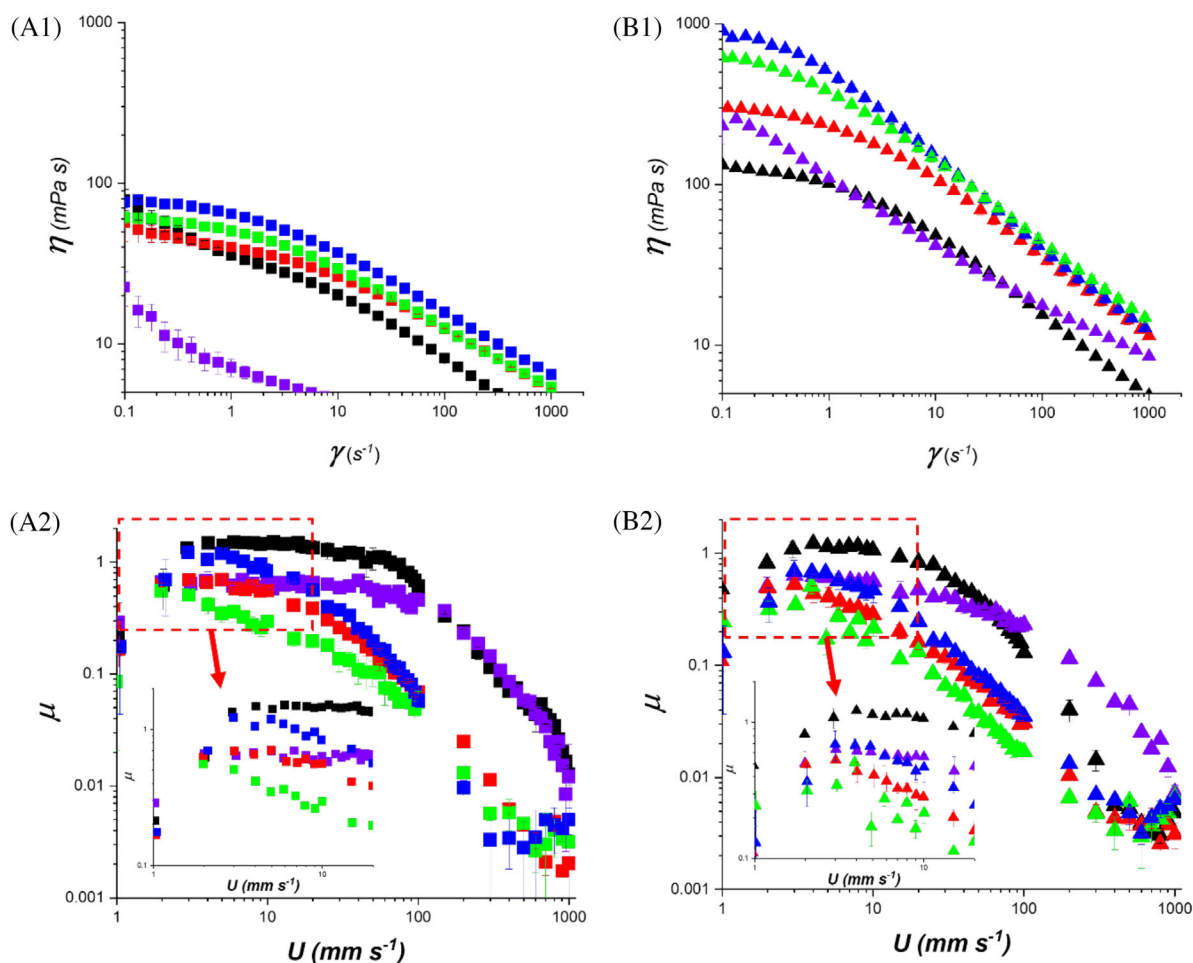
FIGURE 6 Rheological and tribological properties of W/W emulsions. Mean apparent viscosity (η) as a function of shear rate ($\dot{\gamma}$) (A1 and B1) and mean friction coefficient (μ) versus entrainment speed (U) (A2 and B2) of lower concentration (square) with 1.0 wt% GS and 0.1 wt% XG and higher concentration emulsions (triangle) with 2.0 wt% GS and 0.2 wt% XG; GS (Black, ■ or ▲), XG (purple, ■ or ▲), emulsion (red, ■ or ▲), and WPM-loaded emulsion (Blue, ■ or ▲), and PPM-loaded emulsion (green, ■ or ▲), with magnified graph on boundary regime. Error bars represent standard deviations for at least three measurements on experiments performed in triplicates ($n = 3 \times 3$). PPM, protein (pea)-based microgels; WPM, (whey) protein microgels.

to give smaller droplets but with more well-defined spherical shapes. The microscopy results clearly show that the type of microgel added also influences the morphology and structure of the water droplets. In the case of the microgel-laden W/W emulsions, that is, W/W systems with 2.0 vol% WPM or PPM, Figures 6A2 and 6B2 show that the presence of the different types of microgels also influenced the lubrication behavior at both biopolymer concentrations. Specifically, the friction coefficient of the WPM-laden W/W emulsion was higher than the value of $\mu_{emulsion}$ without WPM and even XG alone in the boundary regime ($p < 0.05$) (see statistical differences in Tables S1B and S1C). Earlier it was shown that WPM cannot lower μ_{WPM} in boundary regime as compared to PPM (Figure 3D). Also, Sarkar, Kanti, Gulotta, Murray and Zhang[25] showed that low volume fractions of WPM give relatively poor lubrication properties—because WPM cannot bear the

normal load and overcome the adhesion of PDMS-PDMS surfaces.

The most interesting and unprecedented behavior was shown for μ of the PPM-stabilized droplets, which was lower than $\mu_{emulsion}$ (without PPM or containing WPM) and even XG alone in the boundary regime ($p < 0.05$) (see statistical differences in Table S1). As discussed previously, PPM alone decreased μ significantly in the boundary regime (see Figure 3D), so that this feature was mirrored when PPM was also present in the W/W emulsion system (Figures 6A2 and 6B2). This suggests that both the non-spherical-shaped droplets and/or the presence of soft, adhesive PPM on the surface of these droplets, or in the interstices between them (Figures 5B3 and 5B4), are better able to squeeze into the tribological gap and reduce the friction efficient, as compared to the more spherical and less deformable water droplets stabilized by WPM.

Thus, contrary to expectations, the lubrication performance of the pea protein microgels (PPM) and corresponding PPM-stabilized W/W emulsions was in sharp contrast to the behavior of the parent non-microgelled pea protein,[35,36] which alone is known to increase friction compared to whey protein. This difference is no doubt related to the complex changes in the structure of the pea protein in its conversion to PPM, due to the applied heat and shear.[34,56] PPM indeed showed higher hydrated mass at a gold surface and higher adhesive forces than WPM. In addition, the PPM appeared to stabilize more distorted, non-spherical W/W emulsion droplets which possibly enhanced the lubrication performance of PPM compared to unlike the more typical spherical water droplets stabilized by WPM. Microgel size might also affect lubricity, since the smaller WPM (nearly of half of the diameter of that of the PPM) might be expected to squeeze into the contact region more easily. However, once entrained, the larger volumes (~8x) of the PPM will be able to support more load as compared to WPM. Hence, the differences in lubricity might be related to the PPM being softer than the WPM but also due to the differences in protein affinity, particle size and adhesiveness. We believe that this is the first time that such effects have been reported in the literature.

3 | CONCLUSIONS

Using a comprehensive suite of multiscale techniques, including microscopy, light scattering, rheology, tribology, and surface adsorption measurements, we have demonstrated two key findings. (1) Soft proteinaceous microgels, made from two very different protein sources (pea and whey), can both stabilize Pickering-like water-in-water (W/W) emulsions, though with different morphologies and bulk viscosities. (2) Sustainable plant-based (pea) protein microgels outperform the animal (whey) protein microgels in terms of lubricity on their own as well as the lubricity of the microgel-laden W/W emulsions. Strikingly, the microgel and microgel-stabilized-W/W emulsion performances are in sharp contrast to the behavior of the parent proteins, where pea protein is known to result in increased friction as compared to whey protein. Such differences are attributed to the increased size, lower viscoelasticity, enhanced degree of adsorption, and enhanced adhesive properties of the pea protein microgels as compared to the whey protein microgels. In turn, these microgel differences lead to different morphology of the corresponding Pickering emulsions, the pea protein microgels leading to more distorted, less spherical water droplets which are possibly more easily entrained within the tribological gap. These novel insights pave the way forward for designing water-based sustainable bio-lubricants from plant proteins which should have applications in food, pharmaceutical, personal care and allied sectors. Further development should investigate the sensory response to such systems in order to validate whether the frictional data translates to the oral or skin regimes in terms of mouthfeel or skinfeel.

4 | EXPERIMENTAL SECTION

4.1 | Materials

Xanthan gum (XG, product code G1253, CAS number 11138-66-2), and waxy corn starch (CS, product code 10120, CAS number 9037-22-3) were purchased from Sigma-Aldrich, Dorset, UK. Whey protein isolate (WPI) powder containing 96.3 wt% protein was kindly donated by Fonterra Limited (Auckland, New-Zealand) and commercial pea protein concentrate (PPC) (Nutralys S85XF) with 85% protein content was kindly gifted by Roquette (Lestrem, France). All other chemicals used in the experiments were purchased from Sigma-Aldrich, Dorset, UK unless otherwise specified. MilliQ water purified by a Milli-Q apparatus (Millipore, Bedford, UK), with an electrical resistivity not less than 18.2 MΩ.cm was used as the solvent throughout the experiments.

4.2 | Preparation of hydrogel and microgel particles

Protein hydrogels and microgel particles were prepared using the methods described elsewhere.[3,25,34,37] Briefly, WPI and PPC solutions were prepared by dissolving 12.0 wt% protein (WPI or PPC) in MilliQ water and stirred for 2 hours at room temperature to ensure complete dissolution. Crosslinking to form hydrogels was achieved by heating the whey or pea protein solutions at 90°C for 30 minutes. After cooling to room temperature (22°C), the gel was stored at 4°C for 12 hours. This was followed by blending for 2 minutes with MilliQ water at a 1:5 w w^{-1} ratio of gel to buffer using a hand blender (HB711M, Kenwood, UK). The subsequent dispersion of "coarse" gel fragments was degassed via a THINKY mixer (ARE-250, Kidlington, UK) using a mixing cycle of 2 minutes at 2000 rpm, followed by 1 minute degassing at 2200 rpm. Finally, the dispersion of the gel fragments was homogenized using a two-stage valve homogenizer (Panda Plus 2000; GEA Niro Soavi Homogeneizador Parma, Italy) for two passes, operating at two stages of 250 and 50 bar pressures to form whey protein microgel particles (WPM) and pea protein microgel particles (PPM).

4.3 | Rheology

Samples were studied via a cone-and-plate geometry (CP50-2, cone diameter 50 mm, cone angle 2°, 1 mm gap) in an MCR 302 (Anton Paar, Austria) controlled-stress rheometer. Protein solutions were gelled in situ by performing a temperature ramp (25–90°C at a rate of 0.08°C s^{-1} and held at 90°C for 10 minute), then cooling to 25°C, after which a frequency sweep of 0.1–100 rad/s at a strain of 0.1% was initialized. Due to the long experimental time, the edge of the sample was sealed with a high-viscosity silicone oil (350 cSt) to provide additional protection against sample drying. Strain (γ) sweeps with eight data points per decade of γ, with γ = 0.01–100% were employed. In separate experiments, frequency sweeps were performed after gelation. Frequency sweeps with six data points per decade of frequency (ω) = 100–0.01 rad s^{-1} were employed. Rheological characterization of the biopolymer solutions and water-in-water (W/W) emulsions was performed at shear rates ($\dot{\gamma}$) ranging from 0.1 to 1000 s^{-1} at 37 ± 0.1°C, in order to mimic oral processing conditions. The viscosities of the microgels (WPM and PPM), were also measured at shear rates ($\dot{\gamma}$) ranging from 0.1 to 100 s^{-1} at room temperature. All the experiments were carried out within 2 hours of W/W emulsion formation, during which no visible phase separation of the emulsions had occurred.

4.4 | Atomic Force Microscopy (AFM)

All nanoscale experiments including topographic imaging, nanoscale roughness, and adhesive force measurements of WPM and PPM were carried out with a Multimode 8 AFM on a Nanoscope V controller (Bruker) equipped with a liquid cell. Microgel suspensions were diluted by a factor of 100 using Milli-Q water and 100 μL aliquots were pipetted on to a fresh but untreated silicon wafer substrate. The samples were incubated in a hydrated state for 30 minutes at room temperature and rinsed five times with 100 μL of Milli-Q water using a micropipette to remove non-adsorbed particles that could otherwise adhere to the AFM cantilever tip. Samples were then transferred to the AFM for imaging and kept hydrated at all times. Oscillatory AFM modes such as Peak Force Tapping (at a range of frequencies) and standard liquid Tapping Mode (8–10 kHz) result in highly unstable imaging, presumably due to the soft microgels oscillating in sympathy. Therefore, standard contact mode with very soft cantilevers was used. The probes, MLCT-DC-BIO (Bruker) are also thermal drift compensated which helps to maintain imaging force at the lowest possible force, with Cantilever C being selected, having a spring constant in the range 0.007–0.011 Nm^{-1}.

4.5 | Dynamic light scattering (DLS)

Dynamic light scattering to determine the hydrodynamic microgel particle size was performed using a Zetasizer (Nano ZS series, Malvern Instruments, Worcestershire, UK) A sample of the WPM or PPM dispersion was diluted with MilliQ water solution at a 1: 50 v v^{-1} ratio of microgel particles to water and placed in standard folded capillary electrophoresis cells (DTS1070). Measurements were performed by time-dependent correlation functions, using a detection angle of 173°, and the refractive index of WPM and PPM were set at 1.52 and 1.54, respectively, versus water (1.33). The absorbance of the microgel particles was assumed to be 0.001.

4.6 | Quartz Crystal Microbalance with Dissipation Monitoring (QCM-D)

The adsorption behavior of the microgel particles was measured using Quartz Crystal Microbalance with Dissipation Monitoring (QCM-D, E4 system, Q-Sense, Sweden). In attempting to mimic the adsorption properties of the protein microgel particles (WPM or PPM) at the water-water (W−W) interface, hydrophilic gold-covered sensors (QSX-301, Q-Sense) were used. Frequency (f) as well as dissipation (D) were monitored in real time. All the solutions were injected into QCM-D chamber by a peristaltic pump at a flow rate of 100 μL min^{-1} at 25°C. The first step was to inject Milli-Q water until a stable baseline was observed. The aqueous dispersions of the microgel particles were then injected into the system and left to adsorb under the flow conditions. Each gold sensor was used only once for each experiment. The data were fitted using Voigt model for viscoelastic solids (namely "Smartfit Model") by D find (Q-Sense, Sweden) software to calculate the hydrated mass of the hydrated layers of microgel particles.

4.7 | Preparation of W/W emulsions

Gelatinized starch (GS) (0.2–4.0 wt%) was prepared by dispersing the starch powder in Milli-Q water, followed by heating in an oil bath at 90°C for 15 minutes with constant shearing using an Ultra Turrax T25 homogenizer (IKA-Werke GmbH &Co., Staufen Germany). Xanthan gum (XG) (0.02–0.4 wt%) was dispersed in Milli-Q at pH 7.0 for at least 24 hours at room temperature and then similarly dispersed and heated at 90°C for 15 minutes. Equal volumes of GS and XG dispersions of different concentrations were mixed at 90°C and homogenized at 21,000 rpm for 10 minutes via the Ultra Turrax T25 homogenizer.

For designing Pickering-like W/W emulsions stabilized by microgel particles, WPM or PPM (2.0 vol% in the final mixture, assuming the density of microgels = 1 g mL^{-1}) were added to the XG dispersion before blending the two phases together. This was merely for convenience: adding the microgel particles to either phases (XG or GS resulted in W/W emulsions with similar rheological properties. The W/W emulsions stabilized by microgels showed no signs of phase separation after 4 weeks of storage but the W/W emulsions without microgels showed phase separation after 2 weeks of storage at room temperature (see Figure S7). Hence, all W/W emulsions were measured rheologically and tribologically within a week of formation and were stable, in line with a previous study where W/W emulsions were stabilized by whey protein microgels.[2a]

4.8 | Determination of phase separation and phase diagram

The GS + XG mixtures were stored in 75 × 25 mm flat bottom test tubes sealed with plastic cap and were visually monitored at room temperature for 2 months. To confirm the phase separation accurately, a few mixtures of arbitrarily chosen concentrations were also centrifuged at high speed (20,000 × g) for 30 minutes, at 4°C in Avanti J-30I centrifuge (Beckman Coulter, USA) and the supernatant was collected very carefully. Apparent viscosity measurements were performed via a model MCR 302 (Anton Paar, Austria) shear rheometer, using cone-and-plate geometry (CP50-2, cone diameter 50 mm, cone angle 2°, 1 mm gap) at shear rates ranging from 1 to 100 seconds^{-1}. For each measurement, 2 mL of sample were pipetted onto the plate and a temperature-controlled cover was used to prevent evaporation and maintain the temperature at 22°C. Samples were left on the plate for 2 minutes to achieve thermal equilibrium before rheological measurements commenced.

4.9 | Confocal laser scanning microscope (CLSM)

Samples were visualized using a confocal laser scanning microscope (CLSM, Model LSM 880, Carl Zeiss MicroImaging GmbH, Jena, Germany). Ar/ArKr (488, 514 nm) and He/Ne (543, 633 nm) laser wavelengths were used. 0.5 wt% of Rhodamine B, Acridine orange, and Fast green were dissolved with MilliQ water and the solutions were stored in the dark when not being used. Rhodamine B showed preferential staining of GS ($\lambda \approx 568$ nm, represented as yellow/orange in the images), whilst Acridine Orange ($\lambda \approx 525$ nm, green in the images) and Fast green ($\lambda \approx 633$ nm, green in the images) preferred attaching to

WPM and PPM, respectively. Unlabeled dark areas were therefore assumed to be the unlabeled XG-rich regions. For systems containing microgel particles, it was necessary to wait for 20 minutes to allow any air bubbles to rise out of the samples before they could be poured into the welled slide. A cover slip was then added before imaging.

4.10 | Cryo-scanning electron microscopy (cryo-SEM)

A cryo-scanning electron microscopy (FEI Quanta 200F FEG ESEM, Japan) was used to study the structural features of microgel-loaded W/W emulsion systems following previous methods.[3,22] All samples were first loaded onto rivet sample holders and frozen in liquid nitrogen. The frozen samples were transferred to the cryo-preparation chamber on the SEM, cleaved and etched at −95°C for 4 minutes. Finally, the Pt-coated samples were transferred to the SEM chamber for imaging at −135°C.

4.11 | Tribology of microgel particles and emulsion systems

The lubricating properties of microgels and W/W emulsion samples were measured using a Mini Traction Machine (MTM2, PCS Instruments, London, UK) with PDMS (Sylgard 184, Dow Corning, Midland, MI, USA, base fluid and cross-linker (10:1 w w^{-1})) ball (Ø 19 mm)-on-disk (Ø 46 mm) configuration, with surface roughness, R_a of 50 nm. All the tribological experiments were carried out within 2 hours of preparation of the microgel particles and W/W emulsions, that is, when no visible phase separation had occurred. A normal load (W) of 2 N and a slide-to-roll ratio (SRR) of 50% were set for all measurements. The sliding speeds were varied from 1 to 1000 mm s^{-1}. The coefficient of friction was measured for all samples as a function of entrainment speed. The entrainment speed U is defined as in Equation (1):

$$U = \frac{1}{2}(U_B + U_D) \tag{1}$$

where, U_B is the rolling speed of the ball and U_D is the sliding speed of the disc.

Statistical analyses. All values are reported as the mean and standard deviation of three measurements carried out on at least triplicate samples ($n = 3 \times 3$) prepared on different days. Statistical analyses were carried out using one-way ANOVA and multiple comparison test via SPSS software and differences between samples were deemed significantly different with $p < 0.05$ via Tukey's test.

CONFLICT OF INTEREST STATEMENT

The authors declare no conflict of interest.

DATA AVAILABILITY STATEMENT

The data that support the findings of this study are available from the corresponding author upon reasonable request.

ORCID

Simon D. Connell https://orcid.org/0000-0003-2500-5724

Anwesha Sarkar https://orcid.org/0000-0003-1742-2122

REFERENCES

1. J. Esquena, *Curr. Opin. Colloid Interface Sci.* **2016**, *25*, 109.
2. T. Nicolai, B. S. Murray, *Food Hydrocolloids* **2017**, *68*, 157.
3. K. M. You, B. S. Murray, A. Sarkar, *Food Hydrocolloids* **2023**, *134*, 108009.
4. B. Hazt, H. P. Bassani, J. P. Elias-Machado, J. L. A. Buzzo, J. L. Silveira, R. A. de Freitas, *Food Hydrocolloids* **2020**, *104*, 105769.
5. a) S. Koga, D. S. Williams, A. W. Perriman, S. Mann, *Nat. Chem.* **2011**, *3*, 720; b) A. Perro, N. Coudon, J.-P. Chapel, N. Martin, L. Béven, J.-P. Douliez, *J. Colloid Interface Sci.* **2022**, *613*, 681; c) T.-Y. D. Tang, D. Van Swaay, A. DeMello, J. R. Anderson, S. Mann, *Chem. Commun.* **2015**, *51*, 11429.
6. C. D. Keating, *Acc. Chem. Res.* **2012**, *45*, 2114.
7. a) L.-H. Xue, C.-Y. Xie, S.-X. Meng, R.-X. Bai, X. Yang, Y. Wang, S. Wang, B. P. Binks, T. Guo, T. Meng, *ACS Macro Letters* **2017**, *6*, 679; b) S. C. Silvério, O. Rodríguez, A. P. Tavares, J. Teixeira, E. Macedo, *J. Mol. Catal. B Enzym.* **2013**, *87*, 37.
8. Y. Wang, J. Yuan, Y. Zhao, L. Wang, L. Guo, L. Feng, J. Cui, S. Dong, S. Wan, W. Liu, *CCS Chemistry* **2022**, *4*, 2102.
9. K. R. Peddireddy, T. Nicolai, L. Benyahia, I. Capron, *ACS Macro Letters* **2016**, *5*, 283.
10. Y. Beldengrun, J. Aragon, S. F. Prazeres, G. Montalvo, J. Miras, J. Esquena, *Langmuir* **2018**, *34*, 9731.
11. B. S. Murray, N. Phisarnchananan, *Food Hydrocolloids* **2016**, *56*, 161.
12. H. Khemissi, H. Bassani, A. Aschi, I. Capron, L. Benyahia, T. Nicolai, *Langmuir* **2018**, *34*, 11806.
13. E. Dickinson, *Trends Food Sci. Technol.* **2019**, *83*, 31.
14. A. Sarkar, E. M. Krop, *Current Opinion in Food Science* **2019**, *27*, 64.
15. O. Torres, E. Andablo-Reyes, B. S. Murray, A. Sarkar, *ACS Appl. Mater. Interfaces* **2018**, *10*, 26893.
16. J. R. Stokes, M. W. Boehm, S. K. Baier, *Curr. Opin. Colloid Interface Sci.* **2013**, *18*, 349.
17. J. Chen, J. R. Stokes, *Trends Food Sci. Technol.* **2012**, *25*, 4.
18. a) A. M. Carvalho-da-Silva, I. Van Damme, W. Taylor, J. Hort, B. Wolf, *Food & Function* **2013**, *4*, 461; b) N. Selway, J. R. Stokes, *Food Res. Int.* **2013**, *54*, 423.
19. a) H. J. Lee, R. G. Hollenbeck, J. A. Morgan, A. Kruger Howard, A. Siddiqui, V. A. Sayeed, A. Selen, S. W. Hoag, *Drug Dev. Ind. Pharm.* **2022**, *48*, 198; b) H. Batchelor, R. Venables, J. Marriott, T. Mills, *Int. J. Pharm.* **2015**, *479*, 277.
20. H. Cai, Y. Li, J. Chen, *Biotribology* **2017**, *10*, 17.
21. L. Ma, A. Gaisinskaya-Kipnis, N. Kampf, J. Klein, *Nat. Commun.* **2015**, *6*, 1.
22. F. Xu, E. Liamas, M. Bryant, A. F. Adedeji, E. Andablo-Reyes, M. Castronovo, R. Ettelaie, T. V. Charpentier, A. Sarkar, *Advanced Materials Interfaces* **2020**, *7*, 1901549.
23. M. Nosonovsky, B. Bhushan, Vol. *368*, The Royal Society Publishing, **2010**, 4677.
24. a) Z. Jin, J. Zheng, W. Li, Z. Zhou, *Biosurface and Biotribology* **2016**, *2*, 173; b) G. Limbert, M. A. Masen, D. Pond, H. K. Graham, M. J. Sherratt, R. Jobanputra, A. McBride, *Biotribology* **2019**, *17*, 75; c) A. Mann, B. Tighe, in *Biomaterials and Regenerative Medicine in Ophthalmology*, Elsevier, **2016**, 45.
25. A. Sarkar, F. Kanti, A. Gulotta, B. S. Murray, S. Zhang, *Langmuir* **2017**, *33*, 14699.
26. J. K. Oh, R. Drumright, D. J. Siegwart, K. Matyjaszewski, *Prog. Polym. Sci.* **2008**, *33*, 448.
27. M. Destribats, M. Rouvet, C. Gehin-Delval, C. Schmitt, B. P. Binks, *Soft Matter* **2014**, *10*, 6941.
28. a) T. David-Birman, A. Mackie, U. Lesmes, *Food Hydrocolloids* **2013**, *31*, 33; b) D. Meshulam, U. Lesmes, *Food Function* **2014**, *5*, 65; c) A. Sarkar, V. Ademuyiwa, S. Stubley, N. H. Esa, F. M. Goycoolea, X. Qin, F. Gonzalez, C. Olvera, *Food Hydrocolloids* **2018**, *84*, 282.
29. X. Li, B. S. Murray, Y. Yang, A. Sarkar, *Food Hydrocolloids* **2020**, *98*, 105292.
30. X. Xu, P. Sharma, S. Shu, T.-S. Lin, P. Ciais, F. N. Tubiello, P. Smith, N. Campbell, A. K. Jain, *Nat Food* **2021**, *2*, 724.
31. a) F. Liu, C.-H. Tang, *J. Agric. Food Chem.* **2013**, *61*, 8888; b) F. Liu, C.-H. Tang, *J. Agric. Food Chem.* **2014**, *62*, 2644; c) F. Liu, S.-Y. Ou, C.-H. Tang, *Food Hydrocolloids* **2017**, *65*, 175.
32. B. Jiao, A. Shi, Q. Wang, B. P. Binks, *Angew. Chem.* **2018**, *130*, 9418.
33. a) H.-N. Liang, C.-h. Tang, *LWT-Food Science and Technology* **2014**, *58*, 463; b) Y. Shao, C.-H. Tang, *Food Res. Int.* **2016**, *79*, 64.
34. S. Zhang, M. Holmes, R. Ettelaie, A. Sarkar, *Food Hydrocolloids* **2020**, *102*, 105583.
35. B. Kew, M. Holmes, M. Stieger, A. Sarkar, *Food Hydrocolloids* **2021**, *116*, 106636.

36. M. Zembyla, E. Liamas, E. Andablo-Reyes, K. Gu, E. M. Krop, B. Kew, A. Sarkar, *Food Hydrocolloids* **2021**, *111*, 106364.

37. B. Kew, M. Holmes, E. Liamas, R. Ettelaie, S. D. Connell, D. Dini, A. Sarkar, *Nat. Commun.* **2023**, *14*, 4743.

38. K. M. You, B. S. Murray, A. Sarkar, *J. Texture Stud.* **2021**, *52*, 16.

39. E. Andablo-Reyes, D. Yerani, M. Fu, E. Liamas, S. Connell, O. Torres, A. Sarkar, *Soft Matter* **2019**, *15*, 9614.

40. a) K. Almdal, J. Dyre, S. Hvidt, O. Kramer, *Polym. Gels Networks* **1993**, *1*, 5; b) P. Burey, B. Bhandari, T. Howes, M. Gidley, *Crit. Rev. Food Sci. Nutr.* **2008**, *48*, 361.

41. R. Kornet, C. Shek, P. Venema, A. J. van der Goot, M. Meinders, E. van der Linden, *Food Hydrocolloids* **2021**, *117*, 106691.

42. N. Babault, C. Païzis, G. Deley, L. Guérin-Deremaux, M.-H. Saniez, C. Lefranc-Millot, F. A. Allaert, *J. Int. Soc. Sports Nutr.* **2015**, *12*, 3.

43. A. Sarkar, E. Andablo-Reyes, M. Bryant, D. Dowson, A. Neville, *Curr. Opin. Colloid Interface Sci.* **2019**, *39*, 61.

44. A. Aufderhorst-Roberts, D. Baker, R. J. Foster, O. Cayre, J. Mattsson, S. D. Connell, *Nanoscale* **2018**, *10*, 16050.

45. a) S. X. Liu, J.-T. Kim, *JALA: Journal of the Association for Laboratory Automation* **2009**, *14*, 213; b) G. Dunér, E. Thormann, A. Dědinaitė, *J. Colloid Interface Sci.* **2013**, *408*, 229.

46. D. Graham, M. Phillips, *J. Colloid Interface Sci.* **1979**, *70*, 415.

47. B. S. Murray, N. Phisarnchananan, *Food Hydrocolloids* **2014**, *42*, 92.

48. S. Zhang, B. S. Murray, N. Suriyachay, M. Holmes, R. Ettelaie, A. Sarkar, *Langmuir* **2021**, *37*, 827.

49. a) Q. Xu, B. Qi, L. Han, D. Wang, S. Zhang, L. Jiang, F. Xie, Y. Li, *Lwt* **2021**, *137*, 110421; b) Y. Ji, C. Han, E. Liu, X. Li, X. Meng, B. Liu, *Food Chem.* **2022**, *378*, 132090.

50. S. Saxena, C. E. Hansen, L. A. Lyon, *Acc. Chem. Res.* **2014**, *47*, 2426.

51. S. Wellert, M. Richter, T. Hellweg, R. von Klitzing, Y. Hertle, *Zeitschrift für Physikalische Chemie* **2015**, *229*, 1225.

52. H. C. Shum, A. R. Abate, D. Lee, A. R. Studart, B. Wang, C. H. Chen, J. Thiele, R. K. Shah, A. Krummel, D. A. Weitz, *Macromol. Rapid Commun.* **2010**, *31*, 108.

53. A. Gonzalez-Jordan, T. Nicolai, L. Benyahia, *Langmuir* **2016**, *32*, 7189.

54. M. Vis, J. Opdam, I. S. Van't Oor, G. Soligno, R. Van Roij, R. H. Tromp, B. H. Erné, *ACS Macro Letters* **2015**, *4*, 965.

55. S. Soltanahmadi, B. S. Murray, A. Sarkar, *Food Hydrocolloids* **2022**, *129*, 107660.

56. H. M. Moreno, F. Dominguez-Timon, M. T. Díaz, M. M. Pedrosa, A. J. Borderías, C. A. Tovar, *Food Hydrocolloids* **2020**, *99*, 105375.

SUPPORTING INFORMATION

Additional supporting information can be found online in the Supporting Information section at the end of this article.